DAMAGE DIAGNOSIS USING EXPERIMENTAL RITZ VECTORS

Hoon Sohn* and Kincho H. Law†

ABSTRACT

This paper describes an experimental study on the use of Ritz vectors for damage detection of a grid-type bridge model. A new procedure to extract Ritz vectors from experimental modal analysis is proposed and demonstrated using the test structure. The extracted Ritz vectors are then used for the damage detection of the test structure using a Bayesian probabilistic approach. Using appropriate load patterns, Ritz vectors can be made more sensitive to damage than modal vectors. The results indicate that the use of load-dependent Ritz vectors produce better damage diagnoses than the modal vectors. The Bayesian probabilistic approach is shown to give better diagnostic results than commonly used deterministic methods.

INTRODUCTION

Damage detection and health monitoring of large-scale structures are important challenges to engineering research. One common approach is to employ the vibration characteristics of a structure to predict the damage locations and to estimate the amount of damage [4]. It has been, however, shown that damage in an early stage may not cause significant changes in the modal parameters.

To overcome the sensitivity problems of modal vectors to damage, several alternatives

*Postdoctoral Fellow, Engineering Sciences & Applications Division, Engineering Analysis Group, Los Alamos National Laboratory, Los Alamos, NM 87545, E-mail: sohn@lanl.gov.

†Professor, Department of Civil and Environmental Engineering, Stanford University, Stanford, CA 94305-4020.

have been proposed. Pandey, Biswas, and Samman proposed to compute the mode shape curvature from the displacement mode shape, and demonstrated that the changes in the mode shape curvature can be a good indicator of damage for beam structures [10]. Stubbs, Kim and Topole presented a damage index method to measure the decrease of modal strain energy before and after damage occurrence [16]. Yao, Chang and Lee employed the strain mode shape, which is related to the force redistribution, to identify local damage of a braced steel frame structure [17]. These aforementioned methods require the direct measurement of dynamic strain or the derivative of the measured displacement mode shape to compute the strain mode shape or mode shape curvature. However, the noise induced by the measurement of dynamic strains is generally higher than that from typical accelerometer measurement. Numerical procedures to compute the curvature from displacement also inevitably produce errors.

This paper describes the use of Ritz vectors obtained from imposing different load patterns for damage detection. Ritz vectors have been shown very effective for dynamic and earthquake analyses, eigenvalue problems and model reductions. Recent studies have shown that it is possible to experimentally extract Ritz vectors from the traditional modal analysis [2]. However, very few studies have applied Ritz vectors to damage detection problems [1, 14].

In this paper, Ritz vectors are incorporated into a Bayesian probabilistic framework for damage detection problem [13]. The applicability of this approach is investigated using a grid-type bridge model constructed and tested at the Hyundai Institute of Construction Technology (HICT), Korea. We also present a new extraction procedure of Ritz vectors based on a measured flexibility matrix. The estimated Ritz vectors are then applied to perform the damage diagnosis for the test structure. Finally, the diagnostic results obtained from the Bayesian approach is compared with those by other damage detection methods.

AN EXPERIMENTAL BRIDGE MODEL

The steel bridge model employed in this experimental study consists of two parallel girders and six evenly spaced cross beams connecting the two girders as shown in Figure 1. The girders are steel rectangular tubes and the cross beams are C-shape members. Using impact excitations, we extract Ritz and modal vectors from the vibration response of the test structure.

A SA-390 signal analyzer with four channels is used for the analog to digital conversion of accelerometer signals and the Fast Fourier Transform (FFT) calculation. Data acquisition parameters are specified such that a frequency response function (FRF) in the range of 0 to 100 Hz could be estimated. Each spectrum is computed by averaging three 8 second long time histories. 2048 points are sampled for a 8 second time period and this sampling rate produces a frequency resolution of 0.125 Hz. An exponential window is applied to all measured time histories prior to the FFT calculation.

A Dytran 5801A4 impact hammer and three Dytran 3100B accelerometers with a normal sensitivity of 100 mV/g are used. The excitation is applied at nodes 3, 4 and 5 one at a time as shown in Figure 2. The sensors measure the vertical accelerations at the twelve nodes as indicated in Figure 2.

Note that since the SA-390 data acquisition system has only four channels and there are three accelerometers, the first channel is always connected to the input hammer and the remaining three channels are connected to the three accelerometers. To complete one set of modal test, the hammer excitation is repeated twelve times at one point and the three accelerometers are moved from one set of three nodes to another set of three nodes after every three excitations. (Note that each FRF is computed by averaging the three response time histories, and there are twelve measurement points and three accelerometers.) The rational polynomial [12] technique is employed to extract the first six natural frequencies and the corresponding modal vectors from the recorded FRFs.

EXTRACTION OF RITZ VECTORS

In this section, we present a procedure to extract Ritz vectors from a flexibility matrix constructed using measured vibration data. Following the numerical procedures typically used in generating the Ritz or Lanczos vectors (for example, see References [9] and [2]), the Ritz vectors are computed using the inverse of the stiffness matrix, hereby called the flexibility matrix $\mathbf{F}$, rather than the stiffness matrix itself. It has been shown that a flexibility matrix can be constructed using vibration test data [3]. Thus, it is a natural extension to extract Ritz vectors based on a measured flexibility matrix.

The extraction of Ritz vectors starts with the assumption that the dynamic loading $\mathbf{F}(t)$ can be separated into a spatial load vector $\mathbf{f}$ and time function $u(t)$:

$$\mathbf{F}(t) = \mathbf{f}u(t) \tag{1}$$

If the modal vectors are mass-orthonormalized such that

$$\begin{aligned} \mathbf{V}^T\mathbf{K}\mathbf{V} &= \Omega \\ \mathbf{V}^T\mathbf{M}\mathbf{V} &= \mathbf{I} \end{aligned} \tag{2}$$

the flexibility matrix then can be represented using the modal parameters as [3]:

$$\mathbf{F} = \mathbf{K}^{-1} = \mathbf{V}\Omega^{-1}\mathbf{V}^T \tag{3}$$

where Ω is the spectral matrix with the diagonal entries being the eigenvalues of the system, and $\mathbf{V}$ is the modal matrix for the corresponding eigenvectors. The flexibility matrix can be divided into two parts: the *modal flexibility* $\mathbf{F}_m$, which is formed from the measured frequencies and modal vectors, and the *residual flexibility* $\mathbf{F}_r$ formed from the unmeasured residual modes [3]:

$$\mathbf{F} = \mathbf{F}_m + \mathbf{F}_r = \mathbf{V}_m\Omega_m^{-1}\mathbf{V}_m^T + \mathbf{V}_r\Omega_r^{-1}\mathbf{V}_r^T \tag{4}$$

where the subscripts m and r denote the measured and residual quantities, respectively. Note that the contributions of the lower modes, which are normally estimated in experimental modal analyses, are more significant than those of the higher modes because the contribution of each mode to the flexibility matrix is inversely proportional to the magnitude of the corresponding natural frequency. Therefore, the complete flexibility matrix is approximated by the modal flexibility matrix, *i.e.* $\mathbf{F} = \mathbf{V}_m \Omega_m^{-1} \mathbf{V}_m^T$. It has been reported that the contribution of the residual flexibility is generally about 3-10 % of the modal flexibility matrix [3].

Using the modal flexibility matrix $\mathbf{F}_m$ and the analytical mass matrix $\mathbf{M}$, the first Ritz vector can be computed as:

$$\bar{\mathbf{r}}_1 = \mathbf{F}_m \mathbf{f} \tag{5}$$

where $\mathbf{f}$ is the spatial load distribution vector defined in Equation (1). The first Ritz vector is then mass-normalized as:

$$\mathbf{r}_1 = \frac{\tilde{\mathbf{r}}_1}{[\tilde{\mathbf{r}}_1^T \mathbf{M} \tilde{\mathbf{r}}_1]^{\frac{1}{2}}} \tag{6}$$

The subsequent Ritz vectors are generated using the following recursive relationship:

$$\bar{\mathbf{r}}_s = \mathbf{F}_m \mathbf{M} \mathbf{r}_{s-1} \tag{7}$$

The linear independence of Ritz vectors is achieved using the Gram-Schmidt orthogonalization:

$$\tilde{\mathbf{r}}_s = \bar{\mathbf{r}}_s - \sum_{t=1}^{s-1} (\mathbf{r}_t^T \mathbf{M} \bar{\mathbf{r}}_s) \mathbf{r}_t \tag{8}$$

Finally, the current Ritz vector is mass-normalized:

$$\mathbf{r}_s = \frac{\tilde{\mathbf{r}}_s}{[\tilde{\mathbf{r}}_s^T \mathbf{M} \tilde{\mathbf{r}}_s]^{\frac{1}{2}}} \tag{9}$$

It is worthwhile to briefly compare the flexibility based extraction procedure with the state-space based procedure proposed by Cao and Zimmerman [2]. The state-space

approach requires the information regarding the actual load pattern used in the vibration test. Therefore, the state-space based method only identifies the Ritz vectors corresponding to the specific excitation pattern used in the actual modal testing. Since the spatial load distribution vector $\mathbf{f}$ in Equation (5) can be assigned arbitrary, the flexibility method described here is able to generate different sets of Ritz vectors. Note that both methods require an appropriate approximation for the mass matrix. However, since stiffness changes are the main concern for damage detection problem, the exact estimation of the mass matrix is not necessarily an important issue.

ANALYTICAL MODELING OF THE TEST STRUCTURE

A finite element (FE) model for the grid type bridge structure is constructed using twenty three-dimensional beam elements. As shown in Figure 2, a girder segment between two nodes or a cross beam is modeled as a single element. Fourteen beam elements in the two girders are numbered consecutively from node 1 to node 16. Then, the six cross beams are numbered from left to right. An elastic modulus of 2.0×10^5 MPa, a mass density of 7850 kg/m^3, and a Poisson's ratio of 0.2 are specified for the model. Since the accelerometers measure only the vertical movement of the structure, the lateral degrees of freedom (DOFs) are not included in the analytical model. Therefore, each node of an element has two translational DOFs and three rotational DOFs. The model has a total of 64 DOFs including four rotational DOFs at the boundary. Both ends of the beam are modeled as simple pinned connections. A pinned connection is modeled by a ball bearing with a 35 mm diameter in the experimental setup. Based on a preliminary vibration test, the boundary conditions appear to be less accurately modeled. The boundary conditions are then modified by introducing rotational springs at the rotational DOFs. Furthermore, additional springs are added to the rotational DOFs at both ends of the cross beams to simulate the bolted connection between the girders and the cross beams. After these modifications, the relative errors of the first six natural frequencies between the analytical

model and the test structure fall within 4%.

Table 1 compares the values of the analytical and experimental natural frequencies. Here, the experimental frequency ($\hat{\omega}$) is a mean value of the three frequencies estimated with an impact load applied at nodes 3, 4 and 5, one at a time. Figure 3 displays the analytical and experimental modal vectors of the first six modes. For all figures of modal and Ritz vectors, the structure is viewed from the side.

Figure 4 also shows the first six analytical and experimental Ritz vectors with an impulse excitation at node 3. The experimental Ritz vectors are computed following the extraction procedure descried earlier, and the analytical Ritz vectors are computed using the procedure described in Reference [15]. It should be noted that the first Ritz vector is equivalent to a deflection pattern observed when a unit load is applied to node 3.

As for the scaling of the Ritz or modal vectors, a mass-normalization is conducted. However, since the DOFs of the analytical model do not coincide with the DOFs of the experimental Ritz or modal vectors, a reduced analytical mass matrix is first constructed using the Guyan (static) condensation procedure. Then, both the analytical and experimental vectors are normalized with respect to the reduced mass matrix. Errors arisen from the model reduction are found to be minimum since the inertial forces associated with the omitted rotational and axial DOFs (slave DOFs) are negligible in this example.

A BAYESIAN FRAMWORK FOR DAMAGE DETECTION

A Bayesian framework is applied to diagnose the damages imposed on the test structure [13]. For an analytical model with N_{sub} substructures, the system stiffness matrix $\mathbf{K}$ can be expressed as an assembly of substructure stiffness matrices $\mathbf{K}_{si}$:

$$\mathbf{K}(\Theta) = \sum_{i=1}^{N_{sub}} \theta_i \mathbf{K}_{si} \tag{10}$$

where $\Theta = \{\theta_i; i = 1, ..., N_{sub}\}$ and θ_i $(0 \leq \theta_i \leq 1)$ is a nondimensional parameter which represents the contribution of the ith substructure stiffness to the system stiffness matrix.

A substructure is defined as *damaged* when the θ value is less than a specified threshold.

When vibration tests are repeated N_s times, the total collection of N_s data sets is denoted as:

$$\hat{\Psi}_{N_s} = \left\{ \hat{\psi}(n) \ : \ n = 1, ..., N_s \right\} \tag{11}$$

Each data set $\hat{\psi}(n)$ is composed of the Ritz (or modal) vectors estimated from the nth vibration test:

$$\hat{\psi}(n) = \left[\hat{\mathbf{r}}_1^{nT}, ..., \hat{\mathbf{r}}_{N_r}^{nT} \right]^T \in \mathbf{R}^{N_t} \tag{12}$$

where $\hat{\mathbf{r}}_i^n$ denotes the ith estimated Ritz vector (or modal) in the nth data set $\hat{\psi}(n)$. The vector $\hat{\mathbf{r}}_i^n$ ($\hat{\mathbf{r}}_i^n \in \mathbf{R}^{N_d}$) has components corresponding to the instrumented DOFs. The variables N_t, N_d and N_r represent the total number of components in a data set $\hat{\psi}(n)$, the number of the measured DOFs and the number of the estimated vectors, respectively.

Let H_j denote a hypothesis for a damage event which can contain any number of substructures as damaged. The initial degree of belief about the hypothesis H_j is represented by a prior probability $P(H_j)$. Using Bayes Theorem, the posterior probability $P(H_j|\hat{\Psi}_{N_s})$, after observing the estimated data sets $\hat{\Psi}_{N_s}$, is given as:

$$P(H_j|\hat{\Psi}_{N_s}) = \frac{P(\hat{\Psi}_{N_s}|H_j)}{P(\hat{\Psi}_{N_s})} P(H_j) \tag{13}$$

The most likely damaged substructures are the ones included in the hypothesis H_{max} which has the largest posterior probability, i.e.

$$P(H_{max}|\hat{\Psi}_{N_s}) = \max_{\forall H_j} P(H_j|\hat{\Psi}_{N_s}) \tag{14}$$

Since the objective is to determine the most probable damage hypothesis (event), only the relative posterior probabilities of alternative hypotheses are of interest. We attempt to avoid the explicit expression of a posterior probability $P(H_j|\hat{\Psi}_{N_s})$ since the precise calculation of $P(\hat{\Psi}_{N_s}|H_j)$ is a difficult task. To overcome this difficulty, we focus on the relative comparisons of posterior probabilities.

Note that the search of the most likely damage hypothesis in Equation (14) theoretically requires the examination of all possible damage scenarios. We have proposed a branch-and-bound search scheme using bounding heuristics to expedite the search without exhaustively examining all the possible damage hypotheses [13]. If the damages are localized in a few substructures, the number of damage hypotheses that need to be examined by the branch-and-bound search is relatively small and the search becomes computationally feasible.

DAMAGE DETECTION USING THE EXPERIMENTAL DATA

Continuous deterioration of stiffness is simulated at three different regions of the grid structure and the vibration tests are conducted at six different damage stages as shown in Table 2. The three damage locations (elements 2, 6, and 11) are indicated as shown in Figure 2. First, a single damage is introduced at damage location 1 (for cases 1 and 2) and the second damage is formed between nodes 12 and 13 (for cases 3, 4 and 5). Finally, damage case 6 is simulated by adding damage location 3. For each damage location, a crack is introduced by a saw cutting at a distance of 30 cm to the left of a node as shown in Figure 5. For example, the damage location 1 in Figure 2 is formed at 30 cm left to node 3. The severity of saw cutting in terms of depth (cm) and the percentage ratio of the cut depth to the height of the beam are tabulated as shown in Table 2. Table 3 summarizes the frequencies estimated at each damage stage.

As for comparison, we first present the damage diagnosis results using the six estimated modal vectors. For each damage stage, three sets of modal data, which are obtained from the impulse excitations at nodes 3, 4 and 5, are employed using the Bayesian approach described earlier. The diagnosis results are summarized in Table 4. In the table, the column under $\hat{L}_{dam}$ shows the most likely damaged locations identified by the branch-and-bound search scheme. Since a preliminary sensitivity analysis shows that the measured modal parameters are insensitive to the stiffness changes of the cross beam el-

ements, the branch-and-bound search is conducted including only the fourteen elements within the two girders. The first number in the column "*Rank*" denotes the highest rank among the damage events that include all the actual damage locations, which may also include other "erroneous" damage locations, and the second number presents the rank of the actual damage event. The results show that at the final damage stage the diagnosis employing the modal parameters converges to the actual damage locations.

The same six damage cases are re-diagnosed using the Ritz vectors generated from different load patterns using the measured modal flexibility matrix. A point load is assumed to be applied to the vertical direction of each node and the first six Ritz vectors are generated from each load pattern. This process is repeated for all twelve vertical DOFs and a total of 72 (6 Ritz vectors/load $\times$ 12 load patterns) Ritz vectors are generated. Note that, following the proposed extraction procedure, Ritz vectors corresponding to any load pattern can be theoretically extracted with the same amount of test data used to estimate the modal parameters.

The diagnosis results using the Ritz vectors are also summarized in Table 4. For cases 1 and 2, the actual damage event is ranked as the second and twelfth most likely damage event, respectively. In the first two cases, damage location 1 is included in the most likely damage event estimated by the branch-and-bound search. This is, although the branch-and-bound search fails to pinpoint the actual damage location, the search finds the actual damage location as one of the most likely damage locations. For case 3, the actual damage event is ranked as the ninth most likely event. For case 4, the actual damage case is ranked as the third most likely event. For cases 5 and 6, the branch-and-bound search finds the actual damage events as the most probable ones.

Table 5 shows the first nine most probable damage events identified by the branch-and-bound search for damage case 3. The first two most probable events only include damage location 1 (element 2) and miss damage location 2 (element 11). However, the

third most probable event includes the two damage locations and one extra element 3. That is, although the proposed approach ranks the actual damage event as the ninth most probable event, the third most likely event conservatively includes all the actual damage locations.

The results shown in Table 4 indicate that the Ritz vectors provide better diagnosis results for the six damage cases investigated than the modal vectors. In Figure 6, the sensitivity comparison using the experimental Ritz and modal vectors at different damage stages is conducted. This figure shows the normalized Euclidean norm difference between the "healthy" vectors ($\mathbf{r}^h$ or $\mathbf{v}^h$) and the vector at each damage stage ($\mathbf{r}^d$ or $\mathbf{v}^d$). The Ritz vectors employed for the comparison are those extracted from a point load applied at node 3. It can be seen that a careful selection of load patterns can make damages more observable. The better sensitivity of Ritz vectors to damage locations and the increased amount of information employing multiple load patterns seem to provide better damage diagnosis than using a single invariant set of modal vectors.

Finally, using the test data obtained from case 5, Figure 7 illustrates the branch-and-bound search scheme proposed in Reference [13]. The branch-and-bound search finds the actual damage event as the most likely one after examining 63 different damage scenarios out of 16384 ($=2^{14}$) possible combination of damage scenarios.

COMPARISON WITH OTHER DAMAGE DETECTION METHODS

As for comparison, the Minimum Rank Perturbation Theory (MRPT) [8], damage index method [16], and Sensitivity-Based Element-By-Element (SB-EBE) method [5] are employed in this study.

Minimum Rank Perturbation Theory (MRPT) Method

The MRPT method proposed by Kaouk and Zimmerman consists of two basic steps [8]. First, dynamic residual forces (also know as damage vectors or residual force vectors) are

employed to locate the damaged regions which are mathematically expressed in terms of the DOFs in the analytical model. Second, the lowest rank perturbation is introduced to the analytical stiffness matrix such that the residual forces are minimized. This method is computationally efficient and does not require any iteration. However, the measurement points of the experimental modal vectors should coincide with those of the analytical model, and the dimension of the modal vectors should be the same as the dimension of the analytical model. To satisfy these conditions, the Guyan condensation is applied to the analytical model. The MRPT method can be extended for the case where multiple data sets are available from several static and vibration tests [18].

Using all three modal data sets obtained at each damage stage of the grid structure, Figure 8 summarizes the diagnosis results obtained by the extended MRPT method [18]. In this figure, the abscissa shows the node numbers of the bridge model as defined in Figure 2, and the ordinate displays the changes of the diagonal components of the stiffness matrix at each damage stage. $\mathbf{K}_{ii}^{h}$ and $\mathbf{K}_{ii}^{d}$ denote the stiffness coefficient for node i before and after damage occurrence, respectively. Note that each node has one vertical DOF after the condensation and the stiffness change is normalized such that the maximum change is one. The end nodes for each damaged member are distinguished by darker color in the figure. It can be seen from the results that the damages are not consistently recognized.

Sensitivity Based Element By Element (SB-EBE) Method

The SB-EBE method proposed by Farhat and Hemez searches for the locations of potential errors between the finite element model and the measured modal data, and then update the analytical model at the element level by adjusting the elements' material properties [5]. This method minimizes the squared norms of the modal dynamic residuals via a two-step iteration: At each iteration, the estimated modal vectors are first expanded, and the parameters of the elements are corrected using the expanded modal

vectors and natural frequencies. The SB-EBE method seems to be appropriate here since the mode shape expansion scheme is built within the updating process and damage can be identified at each structural element level. Since this method is designed to employ a single modal parameter set for updating and three sets of modal parameters are experimentally obtained for each damage case, the diagnosis is repeated three times for each damage case. Figure 9 shows the best diagnosis result using three different modal data sets. In this figure, the abscissa represents the element number and the ordinate denotes the percentage change of the corresponding substructure stiffness. It can be observed that the method is partially successful in identifying significant changes in some of the damage locations, but a number of the actual damage locations show very little stiffness changes.

Damage Index Method

The damage index method proposed by Stubbs, Kim and Topole is based on the assumption that the strain energy stored in the structure will decrease in damaged regions [16]. Basically, the damage index for the ith member (β_i) is the ratio of the bending stiffness between the undamaged element (EI_i^h) and the damaged element (EI_i^d):

$$\beta_i = \frac{EI_i^h + 1}{EI_i^d + 1} \tag{15}$$

where a unity value is added to the numerator and denominator to avoid potential numerical problems. This method requires the discretization of the structure into a sufficient number of small elements. Since the bending stiffness EI_i^d term is unknown, the damage index β_i is actually estimated by the curvature of the structure at the ith node. Since the direct measure of the curvature is infeasible, the curvature is approximated as follows [16]: First, the unmeasured nodal amplitudes in the modal vectors are estimated by interpolating the measured nodal amplitudes using a cubic-spline function [11], then a second derivative of the interpolation function is computed at each node. Finally, treating β_i as a realization of a random variable β, a normalized damage index is computed

as follows:

$$Z_i = \frac{\beta_i - \bar{\beta}}{\sigma_\beta} \tag{16}$$

where $\bar{\beta}$ and σ_β denote the mean and standard deviation of the damage indices, respectively. The ith substructure is defined as damaged when $|Z_i| > 2$, which corresponds to a hypothesis testing with 95% confidence level [7].

For the bridge model, each girder is discretized into seventy 7 cm long members and damage locations 1, 2 and 3 correspond to members 16, 56 and 106, respectively. Figure 10 and Table 6 show the diagnosis results using the damage index method. In Figure 10, vertical grid lines are added to display the damage locations for each damage case. In the diagnosis results shown in Figure 10 and Table 6, only the first modal vector is employed since the results are worsened when higher modes are included. This phenomenon is also reported when the damage index method is applied to the I-40 bridge in Albuquerque, New Mexico [6]. It seems quite difficult to approximate the higher modes using numerical interpolations. The results indicate that the damage index method is partially successful in identifying damages near or at the actual damage locations but sometimes fails to detect the damaged members as in cases 5 and 6.

SUMMARY AND DISCUSSIONS

This paper describes the potential application of load-dependent Ritz vectors and their incorporation into the previously proposed Bayesian framework for damage diagnosis. We have also presented a procedure which extracts the Ritz vectors based on a flexibility matrix estimated from experimentally obtained modal parameters. The main advantage of the flexibility based extraction procedure is that the method can generate Ritz vectors from arbitrary load patterns. Damage diagnoses of the grid-type bridge model indicate that the employment of Ritz vectors provides better indication of the actual damage locations than using the modal vectors. The superior performance of Ritz vectors over modal

vectors attributes to (1) the better sensitivity of Ritz vectors over modal vectors and (2) the increased amount of information obtained by employing multiple load patterns.

As for comparison, we also presented the results from the application of the MRPT, SB-EBE, and damage index methods to the test data of the grid structure. The MRPT method requires a decision on the rank of the stiffness perturbation that is added to the original stiffness matrix and the performance of the MRPT method greatly depends on the rank selection. In this study, the rank is decided based on the knowledge of the actual damage locations. However, for real applications, the rank will be selected without the knowledge of damage locations. The SB-EBE method provides better diagnosis result than the MRPT method, and identifies damage amount as well as damage locations. However, the SB-EBE method can only employ one modal parameter set at a time and the diagnosis result varies drastically depending on which modal parameter set is used. Therefore, the SB-EBE method may not be suitable for the continuous monitoring that we are aiming at in this study. The damage index method also provides better diagnosis results than the MRPT method. The advantage of this method is that only a few modes are required to obtain reliable results. In our example, the employment of only the first mode results in the best diagnosis result. However, this method requires the model to be discretized into a large number of small elements. Nevertheless, in this experimental study, the Bayesian approach gives better diagnosis results than the other three methods.

ACKNOWLEDGMENTS

This research is partially sponsored by the National Science Foundation under Grant No. CMS-95261-2. The authors wish to express their sincere thanks to Hyundai Engineering & Construction Co. LTD. for inviting the first author to participate in the test of the grid-type bridge model, and to Dr. Chuck R. Farrar and Dr. Scott W. Doebling of Los Alamos National Laboratory for providing the DIAMOND software. The first author also would like to thank Mr. Jeong Hwan Jang of Seoul National University for

his contributions to the experimental study.

References

[1] T. T. Cao and D. C. Zimmerman. Application of load-dependent Ritz vectors in structural damage detection. In *Proceedings of the 15th International Modal Analysis Conference*, pages 1319–1324, Orlando, FL, 1997.

[2] T. T. Cao and D. C. Zimmerman. A procedure to extract Ritz vectors from dynamic testing data. In *Proceedings of the 15th International Modal Analysis Conference*, pages 1036–1042, Orlando, FL, 1997.

[3] S. W. Doebling. *Measurement of Structural Flexibility Matrices for Experiments with Incomplete Reciprocity*. PhD thesis, Aerospace Engineering Sciences, University of Colorado, Boulder, CO, 1995.

[4] S. W. Doebling, C. R. Farrar, M. B. Prime, and D. W. Shevitz. Damage identification and health monitoring of structural and mechanical systems from changes in their vibration characteristics: A literature review. Technical Report LA-13070-MS, Los Alamos National Laboratory, Los Alamos, NM, 1996.

[5] C. Farhat and F. M. Hemez. Updating finite element dynamic model using an element-by-element sensitivity methodology. *American Institute of Aeronautics and Astronautics*, 31:1702–1711, 1993.

[6] C. R. Farrar and D. Jauregui. Damage detection algorithms applied to experimental and numerical modal data from the I-40 bridge. Technical Report LA-13074-MS, Los Alamos National Laboratory, Los Alamos, NM, 1996.

[7] J. D. Gibson and J. L. Melsa. *Introduction to Nonparametric Detection with Applications*. Academic Press, New York, NY, 1996.

[8] M. Kaouk and D. C. Zimmerman. Structural damage assessment using a generalized minimum rank perturbation theory. *American Institute of Aeronautics and Astronautics*, 32:836–842, 1994.

[9] P. Leger, E.L. Wilson, and R.W. Clough. The use of load-dependent Ritz vectors for dynamic and earthquake analyses. Technical Report UCB/EERC-86/04, Earthquake Engineering Research Center, University of California Berkeley, Berkeley, CA, 1986.

[10] A. K. Pandey, M. Biswas, and M. M. Samman. Damage detection from changes on curvature mode shapes. *Journal of Sound and Vibration*, 145:321–332, 1991.

[11] W. H. Press, B. P. Flannery, S. A. Teukolsky, and W. T. Vetterling. *Numerical Recipes*. Cambridge University Press, New York, 1990.

[12] M. H. Richardson and D. L. Formenti. Parameter estimation form frequency response measurements using rational fraction polynomials. In *Proceedings of the the 1st International Modal Analysis Conference*, pages 167–181, Orlando, FL, 1982.

[13] H. Sohn and K. H. Law. Bayesian probabilistic approach for structure damage detection. *Earthquake Engineering and Structural Dynamics*, 26:1259–1281, 1997.

[14] H. Sohn and K. H. Law. Application of load-dependent Ritz vectors to Bayesian probabilistic damage detection. *Probabilistic Engineering Mechanics*, 1999. (in print).

[15] H. Sohn and K. H. Law. Extraction of Ritz vectors from vibration test data. In *Proceedings of the Second International Workshop on Structural HealthMonitoring*, Stanford, CA, 1999.

[16] N. Stubbs, J. T. Kim, and K. Topole. An efficient and robust algorithm for damage localization in offshore platforms. In *ASCE Tenth Structures Congress*, pages 543–546, San Antonio, TX, 1992.

[17] G. C. Yao, K. C. Chang, and G. C. Lee. Damage diagnosis of steel frames using vibrational signature analysis. *Journal of Engineering Mechanics*, 118:1949–1961, 1992.

[18] D. C. Zimmerman and T. Simmermacher. Model correlation using multiple static load and vibration tests. *American Institute of Aeronautics and Astronautics*, 33:2182–2188, 1995.

Table 1: Comparison of the analytical and experimental natural frequencies

Mode	Frequency (Hz)		Relative
	Analytical (ω)	Experimental ($\hat{\omega}$)	Error* (%)
1st Bending	5.4488	5.5635	2.06
1st Torsion	10.1494	10.0406	1.08
2nd Bending	19.1841	18.6410	2.91
2nd Torsion	30.6216	29.4388	4.02
3rd Bending	41.6086	42.5910	2.31
3rd Torsion	54.9704	57.1864	3.88

* error=$|\omega - \hat{\omega}|/\hat{\omega}$

Table 2: Description for six damage cases of the grid-type bridge structure

Case	Location 1[1]	Location 2[1]	Location 3[1]
1	2.0 cm (40%)	-	-
2	3.0 cm (60%)	-	-
3	3.0 cm (60%)	1.5 cm (30%)	-
4	3.0 cm (60%)	2.6 cm (52%)	-
5	3.0 cm (60%)	3.2 cm (64%)	-
6	3.0 cm (60%)	3.2 cm (64%)	2.5 cm (50%)

1. Damage locations 1, 2 & 3 are shown in Figure 2. The first number is the depth of cut and the second number is the ratio of the cut depth to the height of the beam (5 cm).

Table 3: Natural frequencies (Hz) estimated at different damage levels

Damage case	Natural Frequency (Hz)					
	1st	2nd	3rd	4th	5th	6th
Case 0	5.5635	10.0406	18.6410	29.4388	42.5910	57.1864
Case 1	5.5325	9.8055	18.0557	29.0354	42.0302	56.6170
Case 2	5.4834	9.6725	17.2749	28.5032	41.1840	56.1848
Case 3	5.3699	9.5971	17.2364	27.6911	40.6107	55.3881
Case 4	5.2398	9.5249	17.2193	27.3410	39.7738	52.3992
Case 5	5.0254	9.3938	17.1694	27.1571	38.5939	51.6392
Case 6	4.9622	9.0075	16.1835	26.6957	37.2933	49.9543

Table 4: Damage diagnosis results for the grid-type structure using Ritz & modal vectors

	Damage	Ritz Vectors		Modal Vectors	
Case	Location	$\hat{L}_{dam}$[2]	Rank[1]	$\hat{L}_{dam}$[2]	Rank[1]
1	{2}	{2, 3}	1(2)	{2, 8, 9}	1(29)
2	{2}	{2, 3}	1(12)	{2, 8, 12}	1(46)
3	{2, 11}	{2, 3}	3(9)	{2, 3, 8}	13(41)
4	{2, 11}	{2}	3(3)	{2, 8, 12}	4(12)
5	{2, 11}	{2, 11}	1(1)	{2, 11, 12}	1(9)
6	{2, 6, 11}	{2, 6, 11}	1(1)	{2, 6, 11}	1(1)

1. The first number is the highest rank of a damage event which includes all actual damage locations and the second number in the parenthesis is the rank of the actual damage event.
2. $\hat{L}_{dam}$ is a set of the most probable damage locations identified by the branch-and- bound search.

Table 5: Diagnosis result for damage case 3 of the girder structure

Rank	$\hat{L}_{dam}$	Rank	$\hat{L}_{dam}$	Rank	$\hat{L}_{dam}$
1	{2, 3 }	4	{2, 3, 12}	7	{1, 2, 3}
2	{2, 3, 4}	5	{2 }	8	{2, 12 }
3	{2, 3, 11}	6	{2, 4 }	9	{2, 11 }

Table 6: Actual and estimated damage locations for the damage index method

Case	Members with $\lvert\beta_i\rvert > 2$	Actual damage locations
1	20-26, 34-39	16
2	17-26	16
3	17-24, 101-107	16, 106
4	22-27, 100-109	16, 106
5	20-29	16, 106
6	20-29	16, 56, 106

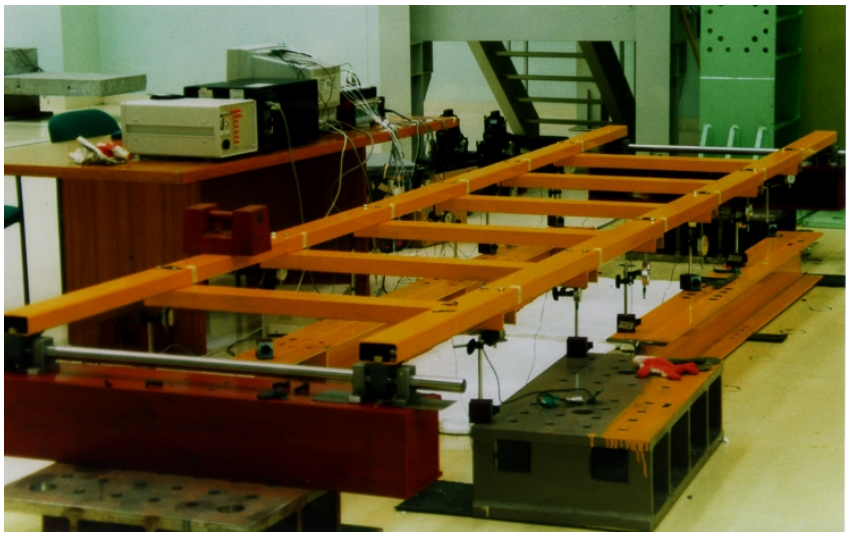

Figure 1: A grid-type bridge model

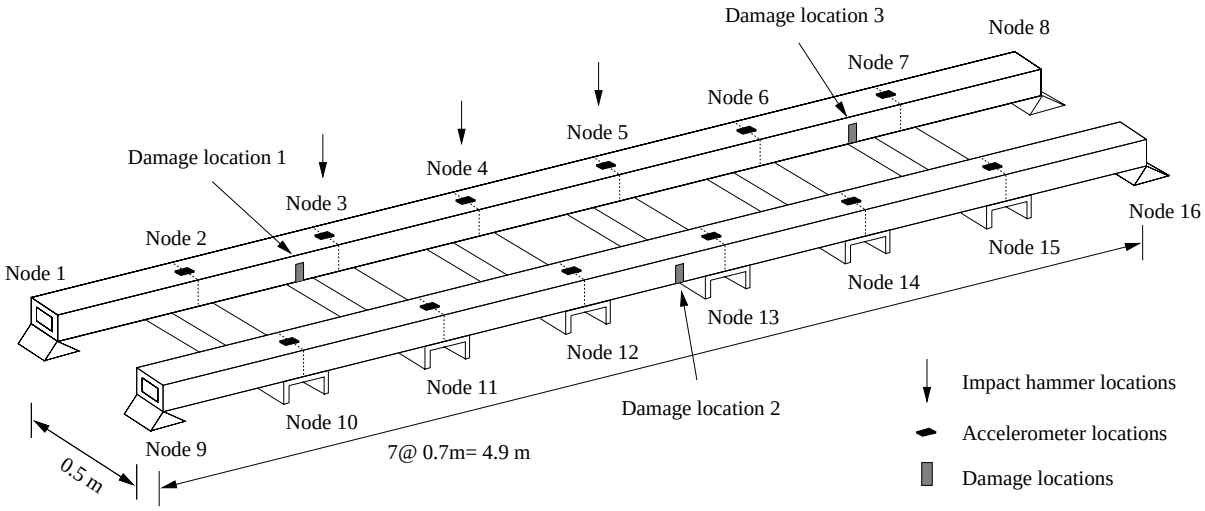

Figure 2: Impact, accelerometer and damage locations of the grid-type bridge structure

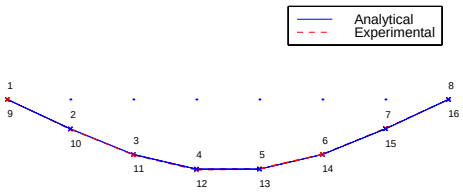

(a) Modal Vector 1

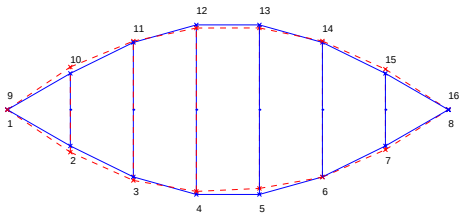

(b) Modal Vector 2

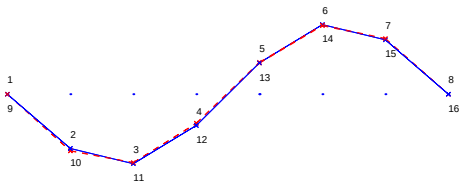

(c) Modal Vector 3

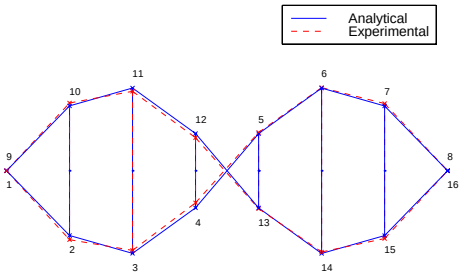

(d) Modal Vector 4

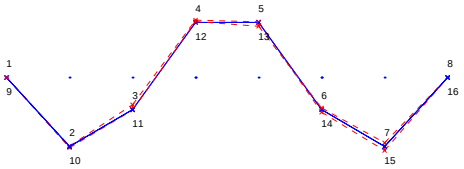

(e) Modal Vector 5

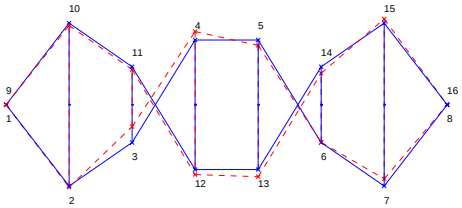

(f) Modal Vector 6

Figure 3: Analytial & experimental modal vectors

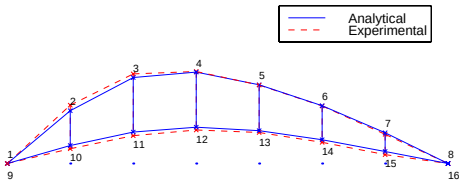

(a) Ritz Vector 1

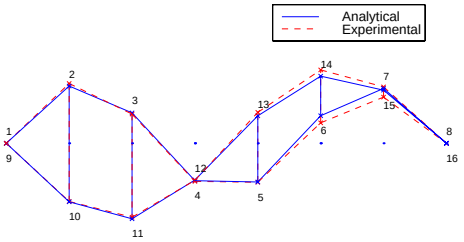

(d) Ritz Vector 4

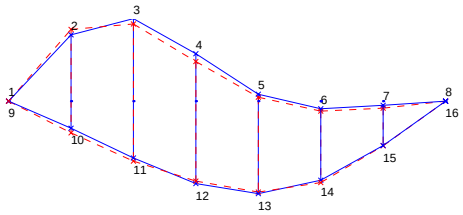

(b) Ritz Vector 2

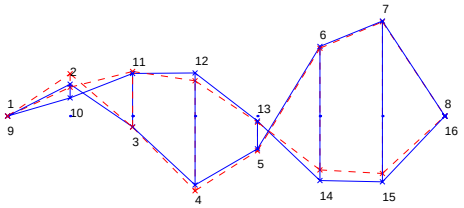

(e) Ritz Vector 5

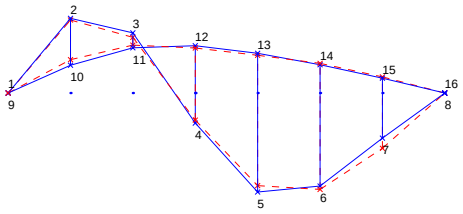

(c) Ritz Vector 3

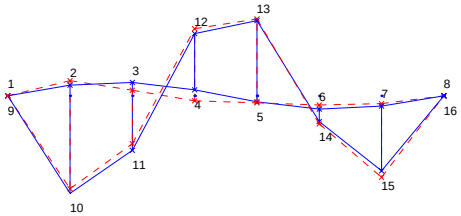

(f) Ritz Vector 6

Figure 4: Comparison of analytical and experimental Ritz vectors

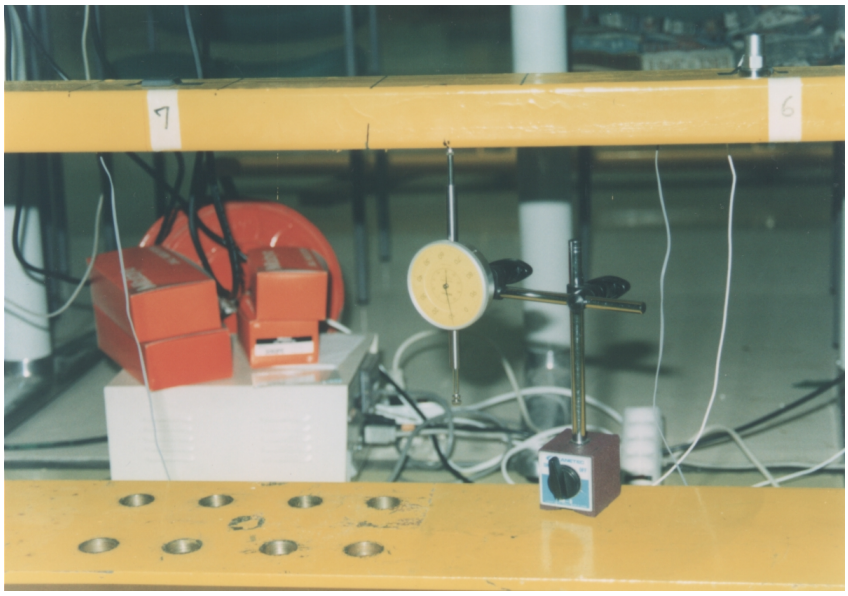

Figure 5: Actual damage introduced to the grid-type bridge structure

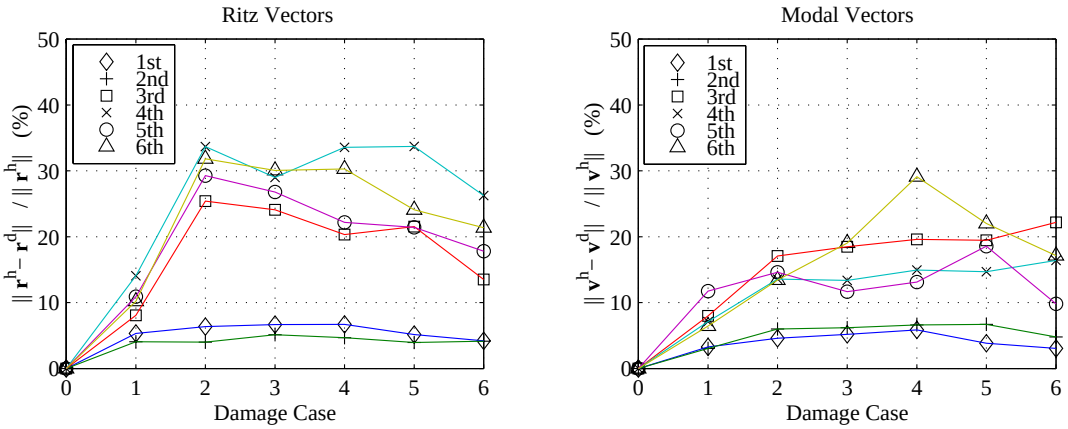

Figure 6: Sensitivity comparison of Ritz and modal vectors at different damage stages

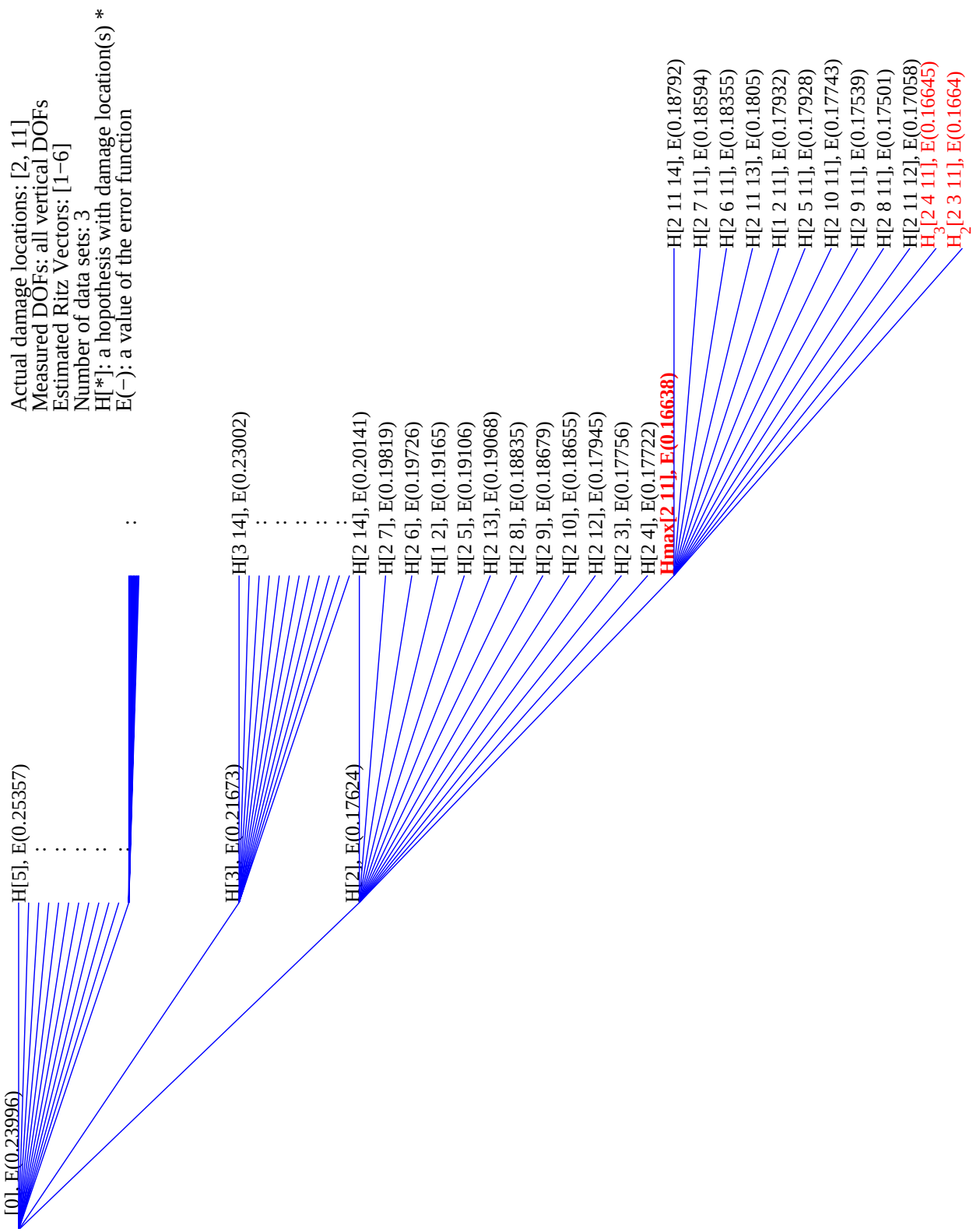

Figure 7: A Branch-and-Bound search of a grid-type bridge model

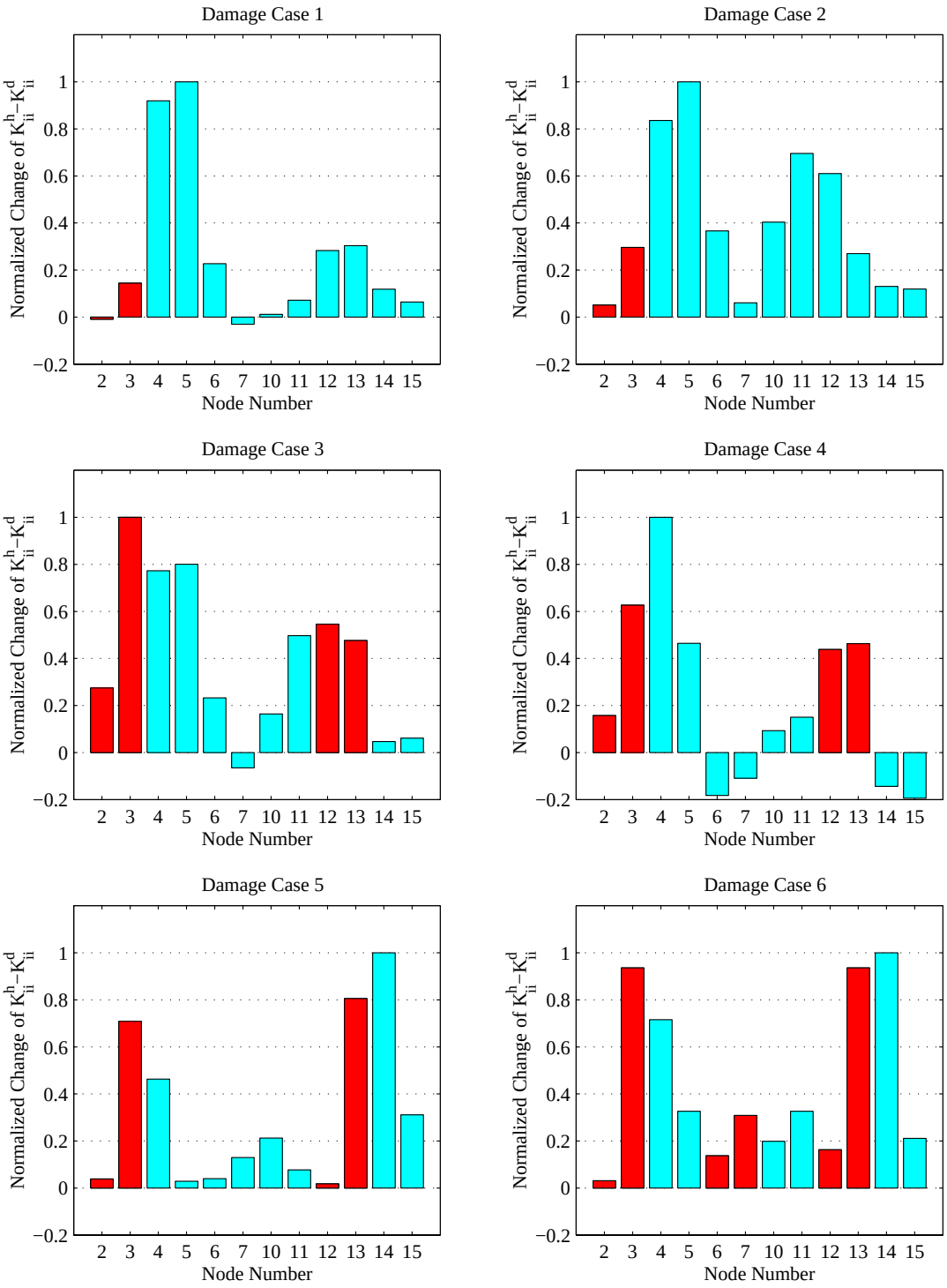

Figure 8: Damage diagnosis of a grid-type bridge model using the MRPT method

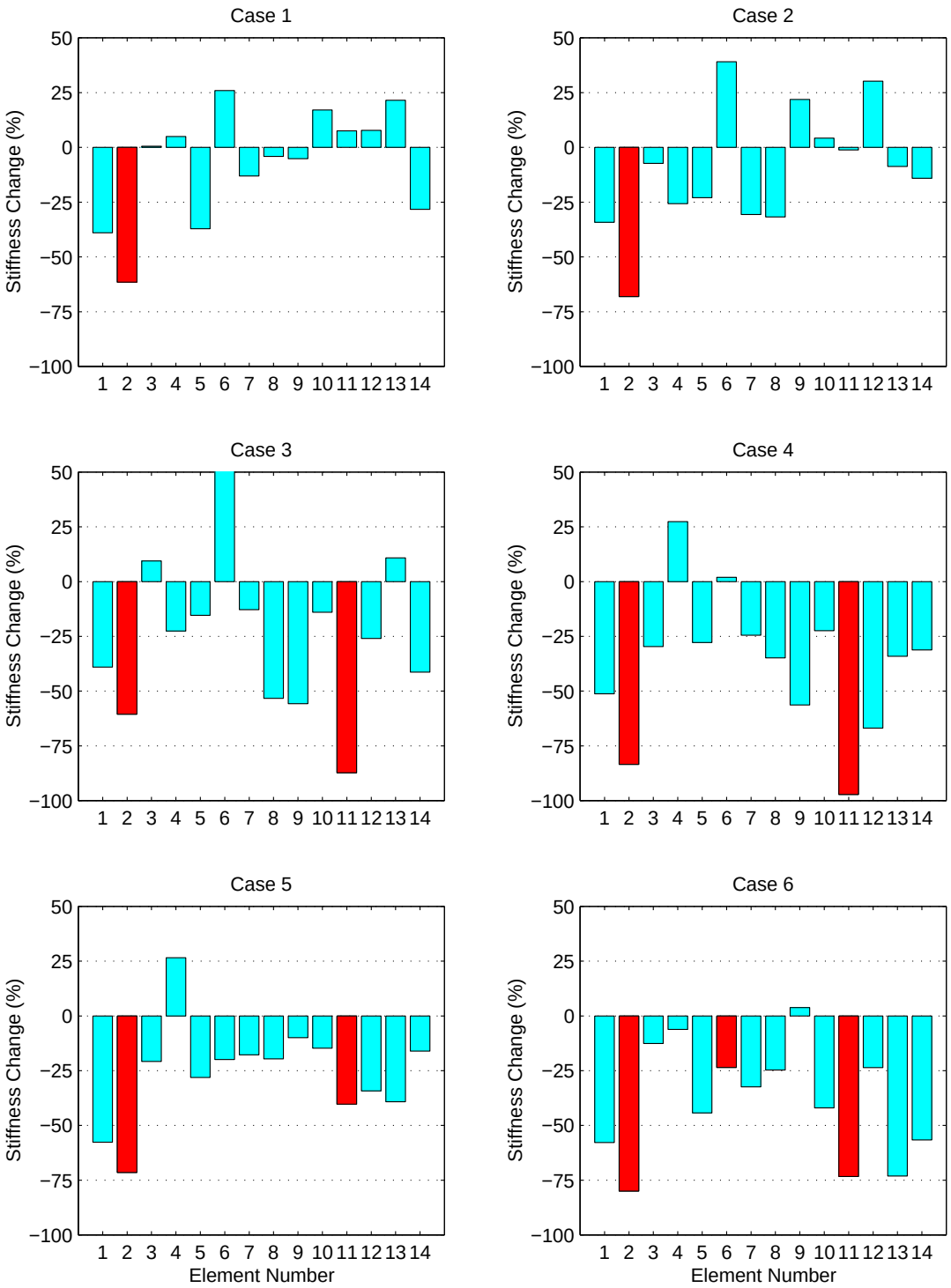

Figure 9: Damage diagnosis of a grid-type bridge model using the SB-EBE method

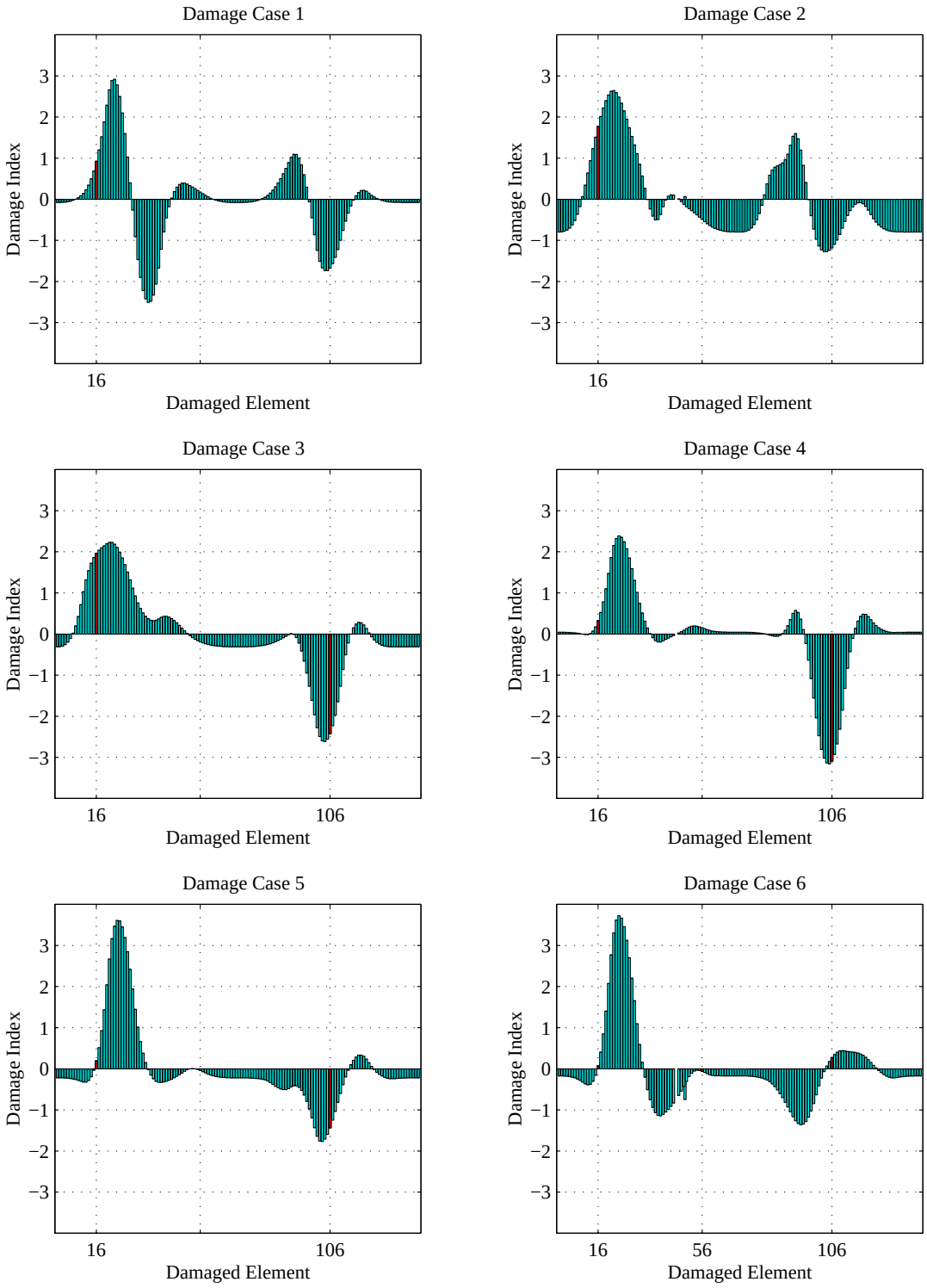

Figure 10: Damage diagnosis of a grid-type bridge model using the Damage Index method